Journal of Renewable and Sustainable Energy

Dominant flow features in the wake of a wind turbine at high Reynolds numbers

Cite as: J. Renewable Sustainable Energy **14**, 033304 (2022); https://doi.org/10.1063/5.0086746
Submitted: 28 January 2022 • Accepted: 03 May 2022 • Published Online: 14 June 2022

A. Piqué, M. A. Miller and M. Hultmark

Journal of Renewable and Sustainable Energy ARTICLE scitation.org/journal/rse

Dominant flow features in the wake of a wind turbine at high Reynolds numbers

Cite as: J. Renewable Sustainable Energy **14**, 033304 (2022); doi: 10.1063/5.0086746
Submitted: 28 January 2022 · Accepted: 3 May 2022 ·
Published Online: 14 June 2022

A. Piqué,[1,a)] M. A. Miller,[2] and M. Hultmark[1]

AFFILIATIONS

[1]Department of Mechanical and Aerospace Engineering, Princeton University, Princeton, New Jersey 08544, USA
[2]Department of Aerospace Engineering, Pennsylvania State University, State College, Pennsylvania 16801, USA

[a)]Author to whom correspondence should be addressed: apique@princeton.edu

ABSTRACT

Dominant flow features in the near and intermediate wake of a horizontal-axis wind turbine are studied at near field-scale Reynolds numbers. Measurements of the axial velocity component were performed using a nano-scale hot-wire anemometer and analyzed using spectral methods to reveal the extent and evolution of the flow features. Experiments were conducted at a range of Reynolds numbers, of $2.7 \times 10^6 \leq Re_D \leq 7.2 \times 10^6$, based on the rotor diameter and freestream velocity. Five different downstream locations were surveyed, between $0.77 \leq x/D \leq 5.52$, including the near wake, transition to the intermediate wake, and the intermediate wake. Three dominant wake features are identified and studied: the tip vortices, an annular shear layer in the wake core, and wake meandering. The tip vortices are shown to have a broadband influence in the flow in their vicinity, which locally alters the turbulence in that area. It is shown that shedding in the wake core and wake meandering are two distinct and independent low frequency features, and the wake meandering persists into the intermediate wake, whereas the signatures of the core shedding vanish early in the near wake.

I. INTRODUCTION

Wind energy is emerging as one of the most successful renewable energy sources when pitted against fossil fuels. The global wind energy sector is aggressively expanding; the estimated compound annual growth rate for offshore wind energy is 31.5% for the period of 2020–2025.[1] Despite this impressive growth, there are still many unanswered questions regarding the flow physics of individual turbines and their integration and collective behavior into wind farms. The wakes of wind turbines are incredibly complex, and their effects on other turbines and the farm as a whole are still not completely understood.[2] Many numerical simulations,[3–7] field campaigns,[8–11] and laboratory experiments[12–15] have been performed to study these flows. However, the flow conditions, in combination with the large length scale characteristic of wind turbines and wind farms, significantly complicate these efforts.[16] Understanding the physics of the flow in the wake of a wind turbine, at the real-world flow conditions, is of utmost importance for our ability to predict, plan, and enhance the overall performance of wind farms.

Environmental conditions are expected to have an effect on wake development such as atmospheric stability, represented through the Richardson number and Obukohv length,[17] large atmospheric boundary layer (ABL) lengthscales,[18] nonuniform flow due to the ABL,[19] and turbulence intensity.[20] The results presented here should be considered idealized with canonical conditions, neglecting many of the added complications of the ABL. Considering a canonical axisymmetric wake generated by a rotor, the flow physics in the wake is primarily governed by two non-dimensional numbers; the Reynolds number, $Re_D = U_\infty D \nu^{-1}$, and the tip speed ratio, $\lambda = \omega R U_\infty^{-1}$, where U_∞ is the freestream velocity, D and R are the rotor's diameter and radius, respectively, ω its angular velocity, and ν is the kinematic viscosity.[21] Their importance in experimental scaling can be seen first in the rotor aerodynamics, which in turn have an effect on rotor performance metrics, such as the thrust coefficient, $C_T = T/(1/2\rho A U_\infty^2)$, and the power coefficient, $C_P = P/(1/2\rho A U_\infty^3)$,[22] although it is also worth noting that C_T has an effect on the wake, namely, in the form of the wake evolution[12] and shape.[23] T is the thrust force on the turbine, A is the area swept by the turbine, $A = 1/4\pi D^2$, ρ is the fluid density, and P is the turbine's power. In order to recreate the flow behind a wind turbine in a wind tunnel using scaled-down models, dynamic similarity must be achieved. This implies that the non-dimensional numbers, as well as the non-dimensional boundary conditions, need to be matched between field and model scales, although Reynolds number invariance of the statistics has been observed to be obtained at Reynolds numbers as low as 100 000.[24] Modern wind turbines have

been growing rapidly in size, and as a result, so have the Reynolds numbers they operate at. Modern offshore machines operate at Reynolds number on the order of $Re_D = \mathcal{O}(10^8)$ and tip speed ratios, $6 < \lambda < 8$. Simultaneous Re_D and λ matching using scaled-down models has not been achieved in laboratory experiments because of the velocities and rotational speeds required to achieve dynamic similarity when the models are scaled down. This is due to the inverse relationship of ω and U_∞ in λ with some authors noting that simultaneous Reynolds number and tip speed ratio matching is impossible in conventional wind tunnels.[21,25,26] With respect to numerical simulations, computational costs are strongly dependent on the Reynolds number, making resolved simulations out of reach for these flows. As a consequence, models are required both to capture the flow physics in the wake and the details of the wind turbines themselves.[27–29] Due to a lack of well-resolved reference data, the accuracy of the models and validity of the assumptions are difficult to evaluate.

The blade level aerodynamics serve as the input to the near wake, a region that is expected to extend two to five diameters downstream of the rotor,[30] which in turn serves as the input to the intermediate and far wakes. As such, understanding the turbine and its wake in detail at all levels is crucial. The blade level aerodynamics of most airfoils can be expected to exhibit Reynolds number effects due to the sensitivity of the transition location and boundary layer condition on the surface.[31] The Reynolds number sensitivity of airfoils has received extensive study with commonly observed effects being an increase in the maximum lift coefficient, C_L, with increasing Reynolds number.[32–36] Other findings showed that an increase in the Reynolds number led to a change in the slope of the C_L curve for small angles of attack, indicating a departure from the thin airfoil theory.[32] Furthermore, it is well known that the Reynolds number dictates laminar to turbulent transition.[37,38] These effects manifest in changes to the boundary layer growth, mean velocity profile, turbulent content, and separation characteristics.[36,39–42] To summarize, the Reynolds number impacts airfoil performance, which in turn affects the flow in the wake. Across the span of the turbine blades, the wakes of individual airfoil sections will be Re_D dependent and will, therefore, lead to a bulk Re_D effect on the near wake of a wind turbine, as has been previously discussed.[31] Even if the Reynolds number effects on individual airfoil sections are fully understood, additional Reynolds number effects may be unknown due to the additional complexities associated with 3D airfoil behavior. Furthermore, wake flow is known to exhibit Reynolds number dependencies, even at relatively large Reynolds numbers, even with a wake generator that is not expected to exhibit any such trends.[43]

Wakes of wind turbines are characterized not only by high Reynolds number turbulence but also by the helical vortex structures that are formed by the tip vortices.[44,45] Tip vortices are shed from each blade and organize themselves in a counter-rotating helical formation, as a consequence of the blade angular velocity and conservation of momentum. The helical tip vortices have been the subject of many studies, but their behavior at high Reynolds numbers and effect on the wake evolution are still poorly understood.[46] In a study (Ref. 47), the tip vortices were shown to introduce a shielding effect that reduces wake growth in the near wake, signaling that additional information on the tip vortex breakdown would be useful for understanding the transition from the near wake. Tip vortex breakdown is thought to be caused by the interaction of the tip vortices in a pairing formation, which can be triggered by fluctuations in the inflow.[48] Although a shear flow, such as that seen in the atmospheric boundary layer, leads to an asymmetric breakdown in the tip vortices, there is no change in the wake's growth rate when compared to an asymmetric wake.[49]

At some downstream distance, the tip vortices breakup and evolve into a single annular shear layer. At this point, the flow transitions to the intermediate wake. The intermediate wake has lost most of the details of the rotor, but the statistics have not yet become self-similar, which is the characteristic feature of the far wake.[50] Self-similar behavior is achieved when the statistical moments collapse when nondimensionalized by the proper length and velocity scales. Therefore, tip vortices and their eventual collapse are important for understanding wake behavior, wake recovery, and the transition from the near to the intermediate wake. However, questions remain regarding the relationship among tip vortex evolution, wake recovery, and Reynolds number.

Another important wake-flow feature is the hub vortex, which is formed through the interactions of the wake generated by the nacelle and the vortices from the blade roots. It has been observed that the hub vortex does not persist as far downstream as the tip vortices, and it is commonly thought of as the weaker structure of the two.[30] Despite its weaker nature and shorter lifetime, the root and hub vortices still play an important role in the wake dynamics. It was shown that the interaction between the tip and hub vortices plays a role in the elusive wake meandering effect[51] and in the reenergization of the wake.[52,53] The wake meandering effect is still a widely debated phenomenon in the wind energy community that has been observed in both field and wind tunnel experiments.[13,52,54] In general, wake meandering is characterized as a low frequency periodic behavior that has been observed in velocity spectra. Proposed explanations for the observed wake meandering effect include atmospheric boundary layer structure convection of the wake and bluff body vortex shedding behavior.[18] The wake meandering signal was first investigated in a wind tunnel experiment (Ref. 13) and can be characterized by the Strouhal number, $St = fDU_\infty^{-1}$, where f is the frequency of the shedding. However, there has been a wide range of reported Strouhal numbers in the literature, ranging from 0.12 (Ref. 13) to 0.28 (Ref. 52).

The study presented herein is based on the same experimental data as were used by the authors in Ref. 50. That study focused on dynamic similarity and scaling of the mean and variance, whereas the present study focuses on the flow structures and spectral analysis of the wake flow.

Nanoscale hot-wire anemometry was used to measure the streamwise velocity in the wake of a model wind turbine across a Reynolds number range of $2.7 \times 10^6 < Re_D < 7.2 \times 10^6$. Since large Reynolds numbers are achieved without large length scales, the smallest length scales are unavoidably very small. To ensure well-resolved measurements, the nanoscale thermal anemometry probe (NSTAP) was used, which yields fully resolved measurements. All tests reported here were performed at a constant tip speed ratio of $\lambda = 5.54 \pm 0.11$. Values for C_T and C_P can be found in Ref. 50, but to summarize these values here, the average $C_T = 0.742$ and average $C_P = 0.352$. Measurements were acquired along horizontal profiles in the spanwise direction for $r/D \leq 0.81$ at streamwise locations between $0.77 \leq x/D \leq 5.52$, ensuring that the near wake and the intermediate wake were surveyed, where the transition between them occurs somewhere between $2.02 < x/D < 3.52$ as reported in Ref. 50.

The identification of dominant flow structures and features in wind turbine wakes has been the subject of several previous numerical, laboratory, and field studies.[11–13,55–62] However, the current work is the first to study such flow structures at near field-scale Reynolds numbers, while also ensuring well-resolved, well-controlled, and well-known flow and operating conditions.

II. EXPERIMENTAL FACILITIES

Here, an overview of the experimental setup is presented. For a more detailed description of the experimental facility, instrumentation, model, and data acquisition system please refer to Ref. 50. The three-bladed HAWT model rotor has a diameter of $D = 0.2$ m and consists of NACA 6 series airfoils. Detailed information regarding airfoil sections and twist can be found in Ref. 63. All experiments were conducted within the High Reynolds number Test Facility (HRTF), which is a high pressure wind tunnel that uses air pressurized up to 238 atm with flow speeds up to 10 m/s, yielding near-field-scale Reynolds numbers. The turbulence intensity of the inflow is kept between 0.51% and 0.73% for all tests with the highest value observed at the highest Reynolds number tested. These turbulence intensity values are not representative of the turbulence levels that a field turbine would see, but should be considered a canonical case. However, by decoupling Reynolds number effects from inflow effects, it enables unique investigations and can serve as a reference case for future studies investigating the effects of inflow conditions on wake evolution.

A custom designed measurement stack was used that consisted of a six-axis load cell (JR3, Inc., model 75E20A4) and a torque transducer (Magtrol, Inc., model TM-305). The model turbine was self-powered and self-starting, so that a magnetic hysteresis brake (Magtrol, Inc., model AHB-3) was used to control the turbine's angular velocity and, hence, the tip speed ratio. However, the self-starting nature of the turbine limits the lower bound of the Re_D operating range, as the turbine is unable to start or measurement uncertainty is increased at low Re_D. Also, the upper bound of the Re_D range was limited due to an increased risk of gear failure at high Re_D. Figure 1 depicts a model of the turbine measurement stack mounted in the HRTF along with the coordinate system used throughout this study. The turbine rotates clockwise. The x direction represents the axial direction, and r represents the radial direction. Please note that a positive r is denoted by the direction shown in Fig. 1, and a negative r is for the opposite direction. A positive and negative r is used so that it is easy to distinguish between the two sides of the measurement plane.

The nano-scale thermal anemometry probe (NSTAP)[64] was used to acquire measurements of the instantaneous streamwise velocity in order to avoid spatial and temporal filtering effects, which would have been present if a conventional hot-wire was used at these high Reynolds numbers, in this facility. Calibration of the NSTAP was conducted before and after every wake dataset using a pitot tube. A temperature correction to the data was determined to be unnecessary, because the change in temperature in between calibrations never exceeded 1.28 °C. The error in the velocity measurements, based on the maximum difference between the pre- and post-calibration datasets, was less than 0.44%.

The NSTAP and the pitot tube were positioned in the freestream during the calibration procedure. The NSTAP's position was controlled via a four-axis traverse. All measurements were acquired on a plane perpendicular to the turbine tower and parallel to the rotor's

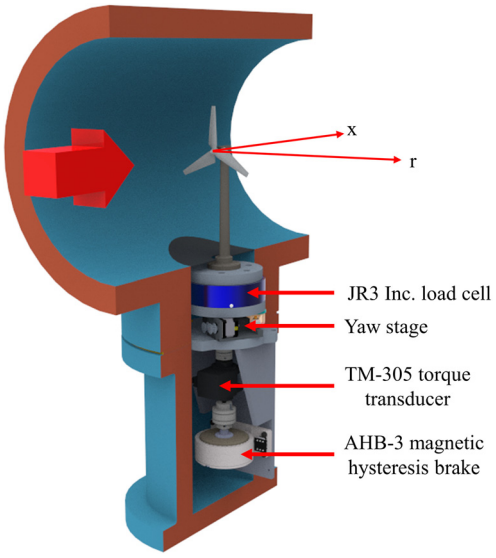

FIG. 1. Turbine measurement stack in HRTF and coordinate system of wake measurements. The large red arrow indicates the direction of flow.

central axis. Data were captured at five different downstream locations, $x/D = 0.77$, 1.52, 2.02, 3.52, and 5.52. A higher point density was deemed necessary for the most upstream location, $x/D = 0.77$, due to the estimated small radial extent of the tip vortex. Therefore, 81 measurements were obtained at $x/D = 0.77$, and 39 measurements were obtained for $x/D > 0.77$, all along the horizontal plane. To validate the level of experimental accuracy maintained in this experiment, premultiplied spectra acquired in the wake of the turbine near the tip vortex and in the core are shown in Fig. 2 for a range of different tunnel pressures, flow velocities, and rotational rates, but at the same Re_D and λ. When non-dimensionalized using the freestream velocity at the specified downstream position, U_e, and rotor diameter, the data collapse very convincingly, certifying the high degree of experimental accuracy and repeatability that was maintained for these hot-wire measurements.

III. RESULTS AND DISCUSSION

A. Signatures of dominant flow features in the wake

In the previous work by the authors, presented in Ref. 50, dominant flow features were identified using a combination of velocity variance profiles, phase averaged velocity, and radial gradients of the axial velocity. The near wake axial velocity deficit and variance profiles are shown in Fig. 3, where tip vortices were identified at the wake's edge for $x/D \leq 2.02$. The streamwise extent of the existence of tip vortices was used to define the end of the near wake to be somewhere in the region $2.02 < x/D < 3.52$. In the near wake, the core exhibited an annular shear layer, which was identified through analysis of the phase averaged data, which indicated a lack of discrete root and/or hub vortices. To give greater insight into these flow features, as well as additional features, an analysis of the spectra will provide detailed information as to the prevalence of certain vortical structures and other flow features, their effect on the surrounding wake flow, as well as the physical phenomena they represent. Here, spectra are obtained

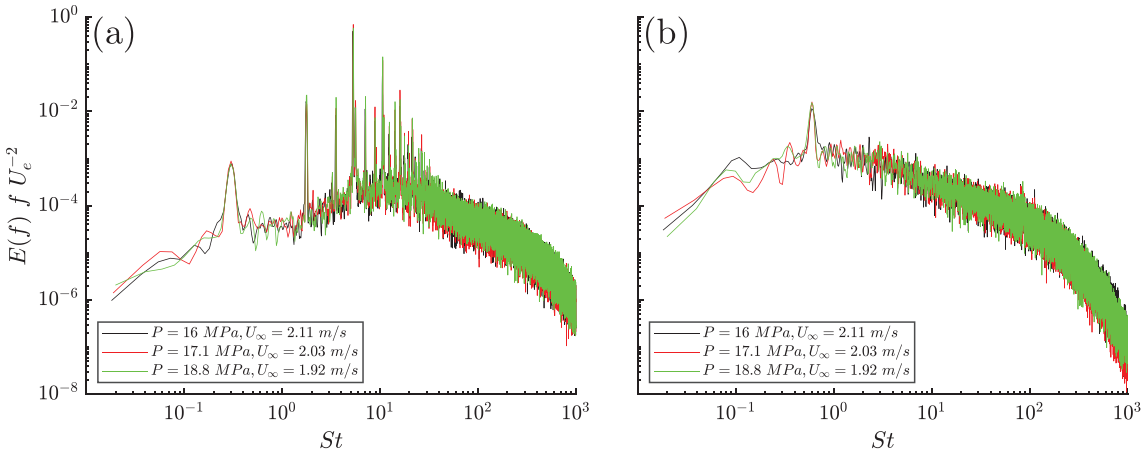

FIG. 2. Pre-multiplied spectra acquired at $x/D = 0.77$, $Re_D = 3.6 \times 10^6$ at different tunnel conditions near the tip vortex location $r/D = 0.526$(a) and in the wake core $r/D = 0.005$ (b). Different combinations of tunnel static pressure, P, and freestream velocity, U_∞, can be used to achieve similar Re_D.

in the form of power spectral density using Welch's method.[65] Evidence of the tip vortices would be expected to show up as a peak in the spectrum at $3f_{rot}$, with f_{rot} equal to the turbine rotation frequency, in the outermost part of the wake, as the rotor has three blades. The annular shear layer in the wake core is not necessarily expected to have a signature in the spectra, apart from a turbulent spectrum, unless it was exhibiting meandering or other kinds of shedding behavior (such as a hub vortex).

Spectral results at Re_D=7.2 $\times 10^6$ for positions near the wake's edge ($r/D = 0.533$) and near the central axis of the nacelle ($r/D = 0.002$) are shown in Figs. 4(a) and 4(b). No significant differences were found for the spectra on the opposite side of the spanwise range surveyed, reinforcing the strong degree of radial symmetry maintained in these experiments. Throughout this paper, the spectra are plotted against the Strouhal number, $St = fDU_\infty^{-1}$, which is the non-dimensional frequency based on the convective timescale. Narrow peaks are found in the spectra from the wake's edge starting at a frequency equal to f_{rot} and then peaks appearing at higher harmonics of that frequency. The peak with the greatest magnitude is found at $3f_{rot}$. A peak at $3f_{rot}$ is expected, as each blade creates one tip vortex. The presence of peaks associated with f_{rot} and $2f_{rot}$ is less expected. It is not clear what the cause for these peaks is, but it could be that one of the blades has a specific signature associated with it. However, the peak associated with $3f_{rot}$ is evidence of the tip vortex, as was shown through phase averaged velocities in Ref. 50, and it has the greatest magnitude of the f_{rot} harmonics. On the wake centerline, there is no evidence of any additional energy associated with f_{rot} as can be seen in Fig. 4(b). In addition to the peaks associated with f_{rot}, two low-frequency peaks can be observed. One around $St = 0.3$, which can be seen in Fig. 4(a) and one around $St = 0.6$, which can be seen in Fig. 4(b). Wake meandering has been shown to correspond to $St = 0.3$ in Ref. 66 and is close to a wake meandering signature of $St = 0.28$,

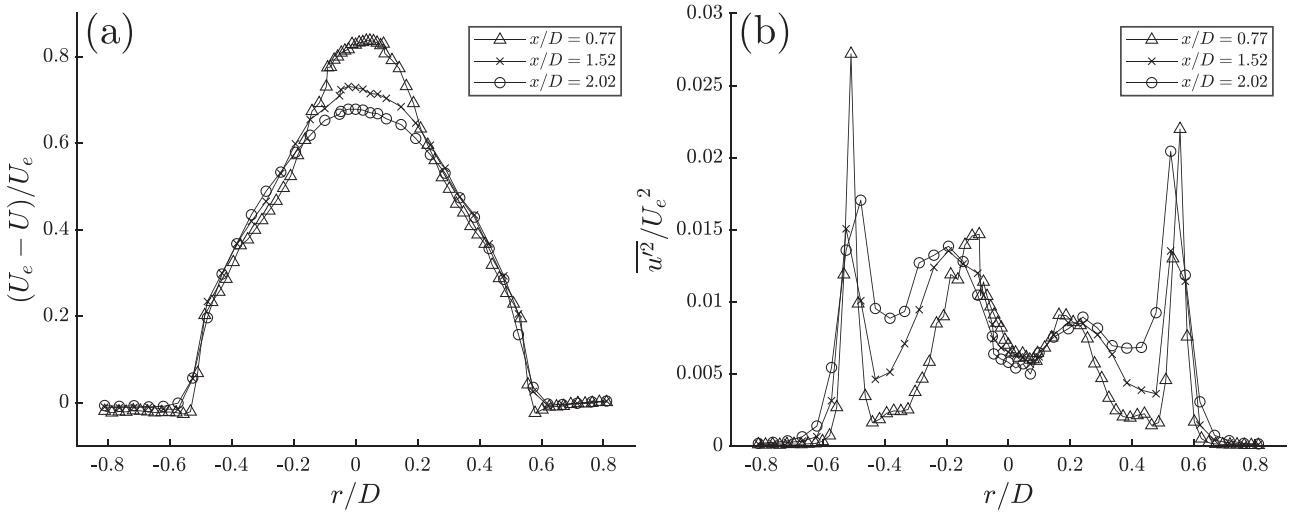

FIG. 3. Axial velocity deficit (a) and axial variance profiles (b) of the presented turbine at $Re_D = 7.2 \times 10^6$ in the near wake, which was found to be for $x/D \leq 2.02$.

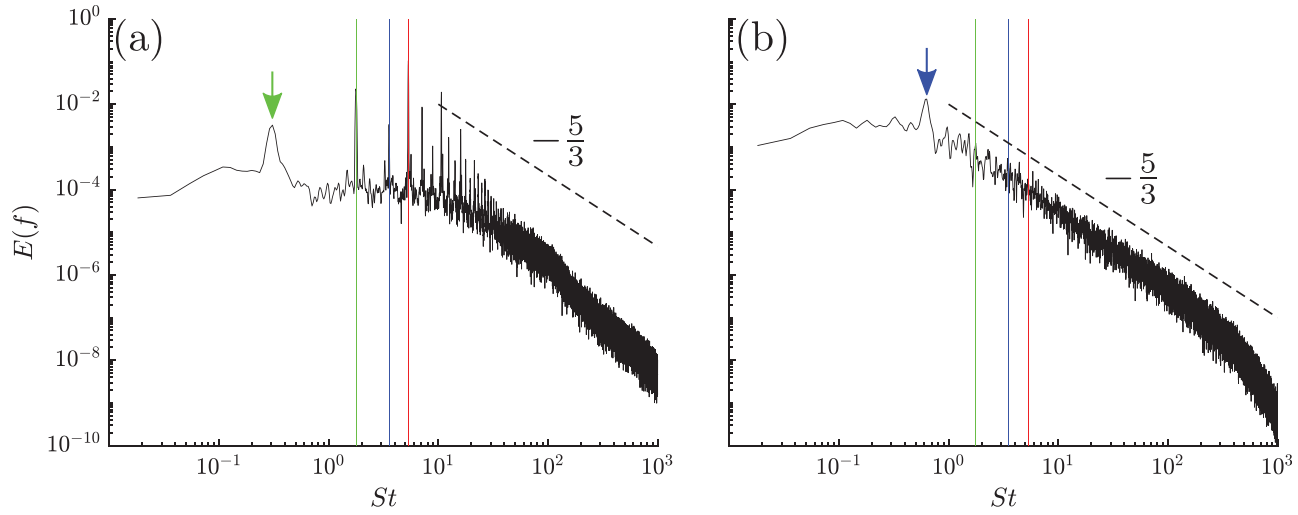

FIG. 4. Power spectral density at $Re_D = 7.2 \times 10^6$ at $x/D = 0.77$ for radial positions $r/D = 0.533$ (a) and 0.002 (b). Green, blue, and red lines represent frequencies associated with f_{rot}, $2f_{rot}$, $3f_{rot}$, respectively. The green arrow calls out the $St = 0.3$ event, and the blue arrow calls out the $St = 0.6$ event.

which was found in Ref. 52. However, the peak at $St = 0.6$ has not been observed before and will be discussed in detail in Sec. III D 1.

The centerline spectrum exhibits a convincing $f^{-5/3}$ region, which spans more than two decades of frequencies, much like one would expect in a canonical turbulent wake at very high Reynolds numbers. In the outer part of the wake, there is no convincing $f^{-5/3}$ region, as the energy associated with the tip vortices pushes the entire spectrum up. Figure 5(a) compares the spectrum at the outer part of the wake for the most upstream and downstream locations. It can clearly be seen that the $f^{-5/3}$ starts to appear first after the tip vortices have vanished, approaching a shape that is very similar to that in the core, Fig. 5(b). This suggests that the effects of the tip vortices are not limited to the rotational frequency and the higher order harmonics but affect the entire turbulence spectrum.

The large range of the $f^{-5/3}$ behavior in the wake core is consistent with the existence of an annular shear layer in that region, indicating that the wake core is free of the effects associated with any surviving root vortices, which must have vanished upstream of

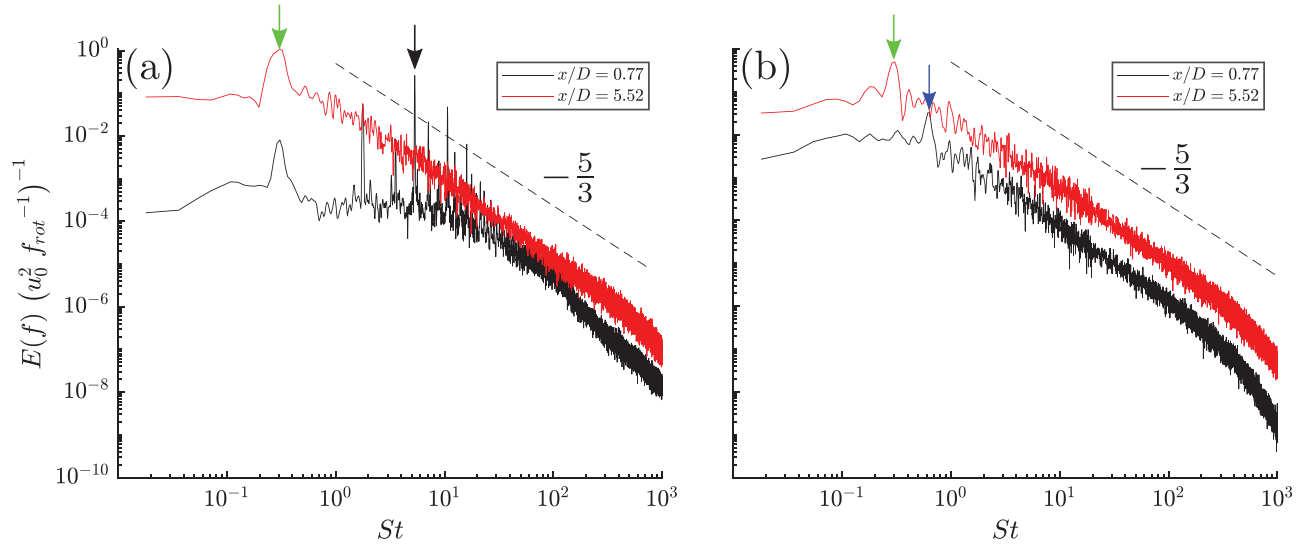

FIG. 5. Power spectral density at $Re_D = 7.2 \times 10^6$ at $x/D = 0.77$ and $x/D = 5.52$. Due to the difference in sample point resolutions between the two downstream positions, there is a small discrepancy in the radial positions. In (a), spectra near the tip vortex are depicted, where at $x/D = 0.77$, $r/D = 0.533$, and at $x/D = 5.52$, $r/D = 0.526$. In (b), spectra near the wake core are depicted, where at $x/D = 0.77$, $r/D = 0.002$, and at $x/D = 5.52$, $r/D = 0.005$. To isolate the differences between the upstream and downstream ranges at the high frequencies, the spectra for $St > 20$ were binned into 40 000 bins. The black arrow calls out the St associated with $3f_{rot}$, the green arrow calls out the $St = 0.3$ event, and the blue arrow calls out the $St = 0.6$ event.

$x/D = 0.77$. This is in agreement with previous studies that have hypothesized that the shear layer is the result of the coalescence of discrete root vortices and shear layers shed from the hub/nacelle.[59,67] To summarize, three dominant periodic structures have been identified in the wake of the presented turbine: tip vortices and two independent low frequency events with St of 0.3 and 0.6. The Reynolds number dependence, spanwise length scales, and downstream evolution of these structures will be discussed below.

B. Reynolds number invariance

Figure 6 shows non-dimensionalized pre-multiplied spectra at the tip and core for two different Reynolds numbers. Interestingly, there is no evidence of any Reynolds number effects on the wake meandering, tip vortices, their higher order harmonics, or the low Strouhal number region in general. There are some Reynolds number effects at the high frequencies, which are to be expected as an increased Reynolds number yields a larger separation of scales and a larger extent of the inertial region. The same observation can be made in the wake core, where the peak corresponding to $St = 0.6$ is unaffected by the Reynolds number with the only discernible effect at the very highest frequencies. Due to the lack of significant Reynolds number effects on the dominant flow features of interest herein, the remainder of this paper will focus on the spectra at the highest Reynolds number, $Re_D = 7.2 \times 10^6$.

C. Visualization of spanwise spectral content

Although the spectra presented in Sec. III A provides detailed information on the most energetic frequencies in the flow, the spanwise distribution and length scales of these features could not be easily determined. To better visualize the spanwise extent of the different flow features, pre-multiplied energy spectra at different radial positions are compiled so that the spanwise extent of dominant periodic structures can be visualized in Fig. 7. The different subfigures correspond to different downstream locations. In these figures, the color represents

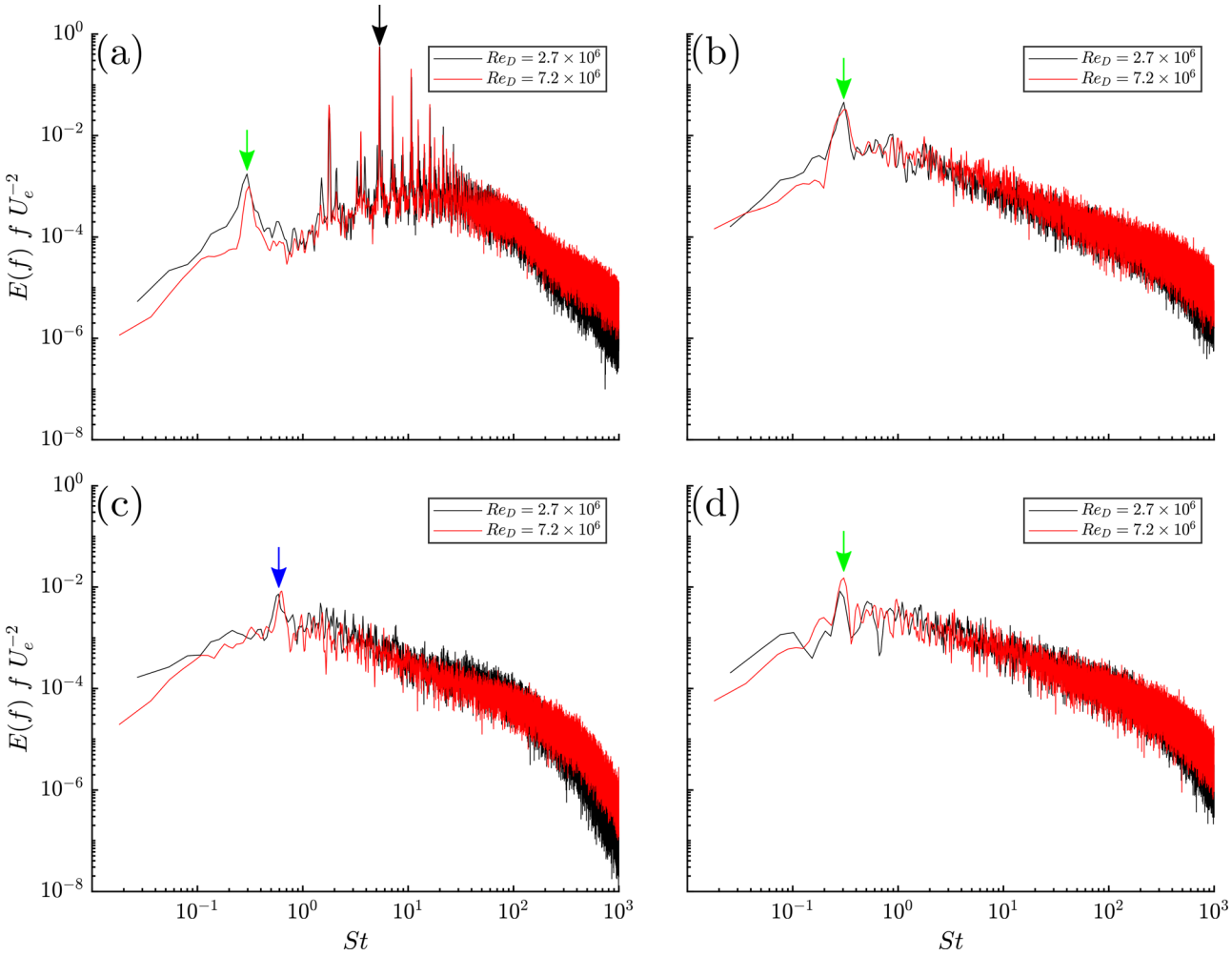

FIG. 6. Premultiplied energy spectrum at $Re_D = 2.7 \times 10^6$ and $Re_D = 7.2 \times 10^6$ near the tip vortex (a) and (b) and near the wake core (c) and (d). Near the tip vortex, $r/D = 0.533$, $x/D = 0.77$ (a), $r/D = 0.526$, $x/D = 5.52$ (b). Near the wake core, $r/D = 0.002$, $x/D = 0.77$ (c), $r/D = 0.005$, $x/D = 5.52$ (d). The black arrow calls out the St associated with $3f_{rot}$, the green arrow calls out the $St = 0.3$ event, and the blue arrow calls out the $St = 0.6$ event.

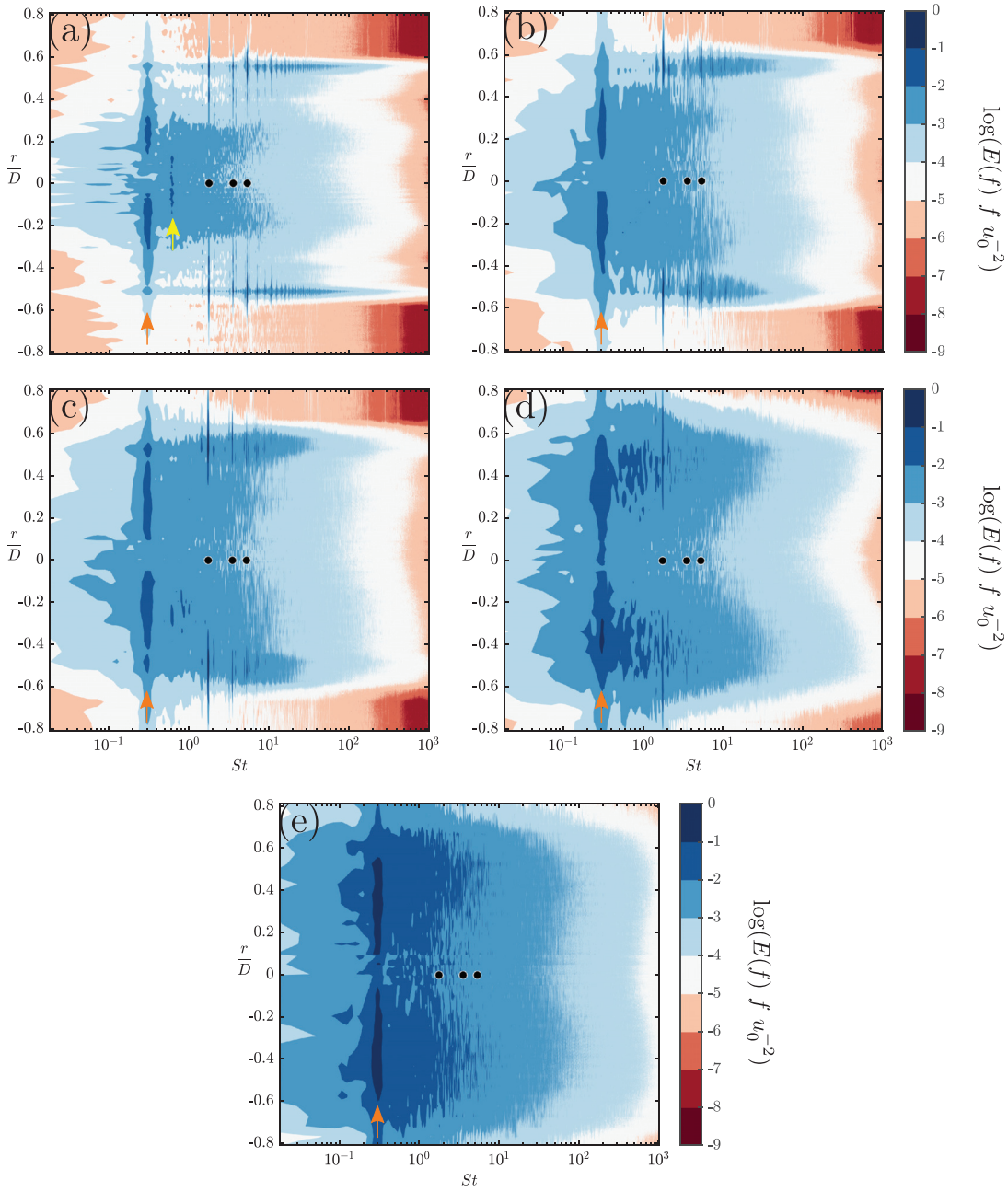

FIG. 7. Premultiplied energy spectrum at Re_D=7.2 $\times 10^6$ at $x/D = 0.77$ (a), 1.52 (b), 2.02 (c), 3.52 (d), and 5.52 (e). Black dots represent frequencies associated with f_{rot}, $2f_{rot}$, and $3f_{rot}$. The yellow arrow indicates the $St = 0.6$ signature, and the orange arrows indicate the wake meandering signature at $St = 0.3$. $E(f)f$ is nondimensionalized by the deficit velocity, $u_0 = U_e - U(r = 0)$.

the magnitude of the premultiplied spectrum, the x-axis is the Strouhal number (non-dimensional frequency), and the y-axis is the radial position. Presentation of the spectra in this manner will be used to further examine wake evolution as it enables identification of different regions in the flow, as well as assisting in identifying characteristic spanwise length scales.

D. Low frequency flow features

Two low frequency peaks can be observed in the spectra in Fig. 7. One at $St = 0.3$, which is seen throughout all tested downstream locations, and another one at $St = 0.6$, which is seen only in the core of the most upstream location. The low frequency event at $St = 0.3$ is

suspected to be a signature of wake meandering as the Strouhal number is close to that found in other previous studies such as $St = 0.28$ in Ref. 52. Reference 68 has suggested that the onset of wake meandering requires a downstream distance of several diameters, because an unstable wake is necessary for wake meandering. Here, it is shown that this is not the case as it is established even at the most upstream location, less than a diameter downstream of the rotor. It is interesting to note that the $St = 0.3$ peak is established long before the tip vortices have vanished. A peak at $St = 0.3$ was expected for the flow near the wake center, as observed in Ref. 69, but interestingly, this is only true further downstream, and it is not until $x/D = 3.52$ the $St = 0.3$ peak spans the entire wake.

The low frequency event identified at the most upstream location, with a higher Strouhal number $St = 0.6$, has not been reported before. Since an annular shear layer has previously been determined to exist in the core of the near wake, the $St = 0.6$ signature may be a characteristic of it. However, the magnitude of the Strouhal number is larger than one would expect to find if this was due to vortex shedding. It is possible that the large Strouhal number is fictitious and that a different length scale better characterizes the low frequency event in the wake's core. The short lived nature of the $St = 0.6$ peak and the fact that the wake meandering signal starts to extend toward the wake center with increasing downstream distance suggest that the annular shear layer in the wake core starts to interact with the outer part of the wake to form a single annular shear layer downstream.

1. Core shedding

Many recent studies would suggest that the low frequency $St = 0.6$ structure is a signature of a hub vortex. Previous laboratory studies,[58,70] stability analysis,[71] and an LES study[68] have made great efforts in understanding the dynamics of the hub vortex, and they have discerned that it can be represented by a helical-like structure in the wake core of their studied turbines. In addition, there are similarities between the studied turbine and the previous studies. For example, in Ref. 58, the nondimensional frequency, f_{hub}/f_{rot}, is equivalent to 0.34, and for the turbine of this study, it is 0.35. However, the wake core structure observed in this study has other unique features. In the studies of Refs. 58, 70, and 71, only a single low frequency structure was observed in their studied wakes and was thought to be caused by the hub vortex. For the studied turbines, two low frequency structures were observed at the same downstream location. Furthermore, the study of Ref. 68 concluded that the breakdown of the unstable hub vortex gave way to wake meandering. No such conclusion can be made for the turbine of this study, as the wake meandering and wake core structures exist at the same downstream location of $x/D = 0.77$. Therefore, it cannot be concluded that the wake core structure observed for the measured turbine is the same hub vortex that was found in the aforementioned efforts.

Here, we hypothesize that it instead is conventional bluff-body shedding that is responsible for the $St = 0.6$ signature, and it is created by only the innermost part of the rotor. This results in the presence of a different length scale, which can explain why the $St = 0.6$ region overlaps, almost perfectly, with the region where the wake meandering behavior is absent in Fig. 7(a). The $St = 0.6$ peak is found for $-0.05 < r/D < 0.14$ at $x/D = 0.77$, while the spanwise extent of the root is $-0.074 < r/D < 0.074$. Using the spanwise extent of the $St = 0.6$ core region, $r/D = 0.28$, as the characteristic length, l_{core}, a different Strouhal number can be defined for this peak, $St_{core} = 0.17$. In classical solid disk wake experiments, shedding has been characterized by $St = 0.135$,[72–74] and in another study, (Ref. 75), the shedding was classified by $St = 0.15$. In porous disk studies, shedding has been characterized by similar Strouhal numbers, $St = 0.15$, with vortex shedding being the most evident for porous disks with high solidity.[75] The $St_{core} = 0.17$ is close to the expected values of porous and solid disks, which suggests that the core of the turbine may be acting like that of a high-solidity porous disk, such that there is core shedding. The disk-like behavior of the wake could be supported by the high solidity, σ, of the turbine's core, which is due to the large chord length of the model used in this study. σ is the ratio between the area occupied by the turbine, including the hub, to a set radius and the area swept by the turbine to the same set radius. The solidity of the $St = 0.6$ region of $-0.14 < r/D < 0.14$ is $\sigma = 0.654$. Reference 75 showed that classical solid disk shedding was not present for porous disks with low solidity but hypothesized that for porous disks with a minimum critical solidity, σ_{crit}, classical solid disk shedding would be present. The range for this critical solidity was $0.6 < \sigma_{crit} < 0.85$. The calculated $\sigma = 0.654$ of the $St = 0.6$ region fits within this range. The tip speed ratio of this experiment was also relatively high, and it has been suggested that high tip speed ratios tend to make turbines act as if the solidity is higher.[59] A combination of high solidity, high tip speed ratio, and a lack of evidence for the presence of discrete root vortices leads to the conclusion that the wake core in the near wake is characterized by an annular shear layer with bluff body-like shedding. In addition, these findings indicate that the previously chosen l_{core} can be seen to represent the diameter of a porous disk.

The aforementioned conclusion suggests that there are two independent low frequency events: one restricted to the wake's core and the other is the wake meandering phenomenon that occupies the majority of the wake. The presence of two low frequency structures implies that one must be careful in how to characterize the wake meandering phenomenon in the near wake, as the wake core shedding may lead to misleading conclusions. For example, a common technique for measuring the wake meandering using flow visualization is to map out the instantaneous point of minimum velocity in the wake.[51,76] From the current study, we know that such a technique would incorrectly be mapping the core shedding instead of the meandering, at least in the near wake.

E. Distribution of dominant vortical structures in the near and intermediate wake

In the near wake, $0.77 \leq x/D \leq 2.02$, Figs. 7(a)–7(c), there are large narrow peaks at frequencies associated with the harmonics of the turbine's rotation rate as discussed in Sec. III A. Another interesting observation is that the energy content around the tip vortices extends across a much larger frequency range than is observed for other flow regions. This observation is true for all downstream locations but most prominent at the most upstream location. Another implication of the broadband nature of the tip vortices is that generalized Joukowsky models, such as those of Refs. 77 and 78, which tend to represent the tip vortex as the only dominant structure in this region of the flow, might not capture this effect.

To better understand the effect that downstream distance has on the energy distribution associated with the tip vortices and the annular

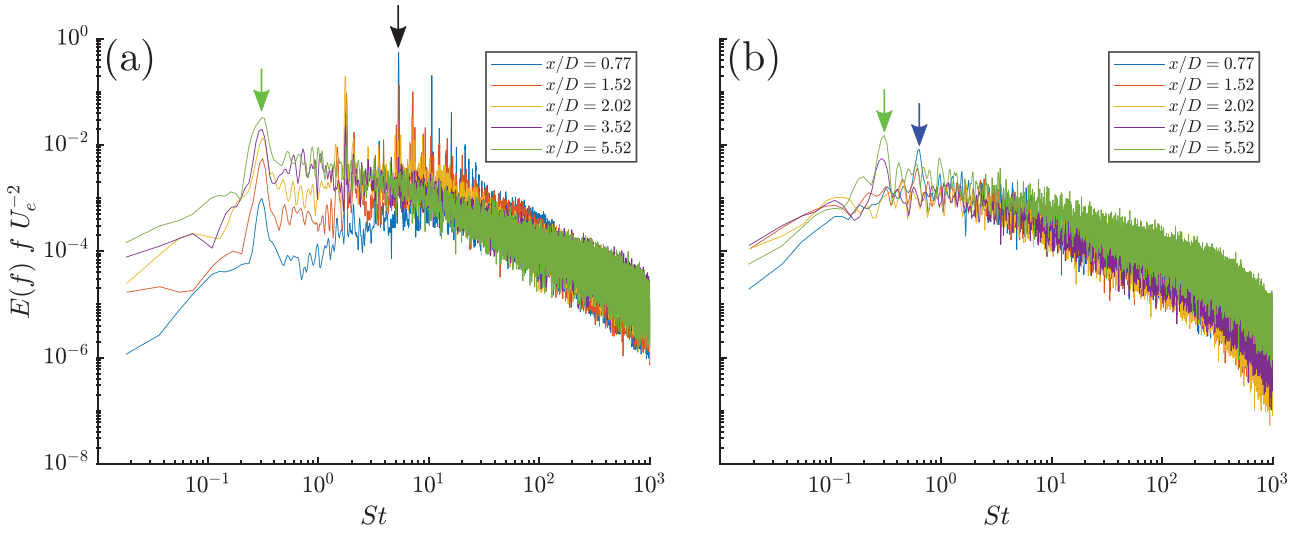

FIG. 8. Premultiplied energy spectrum at Re_D=7.2 $\times 10^6$ at 0.77 $< x/D <$ 5.52 near the tip vortex (a) and near the wake core (b). In (a), the spectrum at $x/D = 0.77$ is at $r/D = 0.533$, and the spectrum at $x/D > 0.77$ is at $r/D = 0.526$. In (b), the spectrum at $x/D = 0.77$ is at $r/D = 0.002$, and the spectrum at $x/D > 0.77$ is at $r/D = 0.005$. The black arrow calls out the St associated with $3f_{rot}$, the green arrow calls out the $St = 0.3$ event, and the blue arrow calls out the $St = 0.6$ event.

shear layer in the wake core, the premultiplied spectrum near the tip vortex is presented in Fig. 8(a). From Fig. 7, it can be seen that with increasing downstream distance, the peak magnitudes associated with the flow near the tip vortex decrease and the high frequency extent of that region decreases due to viscous dissipation and wake recovery. In Fig. 8(a) that trend is shown by the decrease in the magnitude of the higher order harmonics of f_{rot} with increasing downstream distance.

The collapse of the tip vortices can be seen to occur around $x/D = 3.52$ [Fig. 7(d)], consistent with the observations in Ref. 50 where a four-peak profile of the variances transitioned to a two-peak profile around the same downstream location. It can be observed that this transition is also marked by a general change in the shape of the spectrum in Fig. 8(a), where the region between the energetic core and the tip vortices is slowly being energized to engulf the entire wake. This observation is likely the signature of the wake transitioning to a more classical axisymmetric wake.

From Fig. 8(b), there is no obvious downstream evolution of the wake core except for the presence of a low frequency signature at $St = 0.6$ for $x/D = 0.77$, which is absent further downstream. At $x/D \geq 3.52$, the wake meandering signature, found at $St = 0.3$, is present throughout the span of the wake, and its magnitude continues to increase. Unlike in the tip vortex region, there is no distinct feature distinguishing the near and intermediate wake in the core. This supports the previous conclusions made in Ref. 50 that a more rapid transition to intermediate wake behavior is observed in the wake core.

IV. CONCLUSIONS

The dominant flow features in the wake of a wind turbine are studied in the near and intermediate wake at near-field-scale Reynolds numbers. The application of nano-scale hot-wire anemometry reduced any spatial and temporal filtering effects on the data due to the high Reynolds numbers. Spectral analysis in the form of PSD and premultiplied spectrum aided the discussion on the identification of flow features, their downstream evolution, and the mechanisms giving rise to them. Overall, tip vortices, wake meandering, and a low frequency shedding event in the wake's core were found to dominate the wake. Over the limited Re_D range shown here, there were no distinguishing Re_D effects on the spectral signatures of any of these flow features, except for at the extension of the inertial subrange and dissipation scales. This observation agrees with the previous findings of Re_D invariance.[24,79] However, for quantities that are more sensitive to blade sectional drag, such as C_P, it appears that field scale Reynolds numbers are still required.[63]

As has been found in recent wake studies, the tip vortices play an important role in the outer part of the wake, and signatures associated with higher order harmonics of the turbine's rotation rate were shown to affect the entire turbulent spectrum. With increasing downstream distance, the tip vortex signature and the signatures of the higher order harmonics decrease in relative magnitude and vanish entirely within the region of $2.02 \leq x/D \leq 3.52$.

Clear signatures of wake meandering, although still a contentious topic in the wind energy community, were found at $St = 0.3$. Wake meandering was found to be present at less than one diameter downstream of the turbine, despite previous results arguing greater distances are required. This low frequency structure was present throughout the near and intermediate wake; however, it was not present in the wake core at the most upstream location of $x/D = 0.77$. Instead, a different low frequency event, at $St = 0.6$, was found to be present in the wake core at $x/D = 0.77$. In addition, the spectra in the wake core experience little change in the transition from the near to the intermediate wake, suggesting that near wake structures, such as discrete root vortices, experienced a rapid collapse, hastening the transition to intermediate wake behavior in the core. It was found that when the spanwise extent of the annular shear layer was used to form the Strouhal number, instead of the rotor diameter, the Strouhal number of the peak is $St_{core} = 0.17$, on the order of what is expected for bluff-body or high

solidity porous disk shedding. It was also shown that the radial extent of the wake core signature was consistent with the region of the turbine with high enough solidity to expect such shedding.

ACKNOWLEDGMENTS

The authors would like to acknowledge the support of the National Science Foundation under Grant No. CBET 1652583 (Program Manager Ron Joslin).

AUTHOR DECLARATIONS

Conflict of Interest

The authors have no conflicts to disclose.

DATA AVAILABILITY

The data that support the findings of this study are available from the corresponding author upon reasonable request.

REFERENCES

[1]Global Wind Energy Council, "GWEC Global Wind Report 2021" (2021).
[2]P. Veers, K. Dykes, E. Lantz, S. Barth, C. L. Bottasso, O. Carlson, A. Clifton, J. Green, P. Green, H. Holttinen *et al.*, "Grand challenges in the science of wind energy," Science **366** (2019).
[3]J. F. Ainslie, "Calculating the flowfield in the wake of wind turbines," J. Wind Eng. Ind. Aerodyn. **27**, 213–224 (1988).
[4]J. N. Sorensen and W. Z. Shen, "Numerical modeling of wind turbine wakes," J. Fluids Eng. **124**, 393–399 (2002).
[5]M. Calaf, C. Meneveau, and J. Meyers, "Large eddy simulation study of fully developed wind-turbine array boundary layers," Phys. Fluids **22**, 015110 (2010).
[6]Y.-T. Wu and F. Porté-Agel, "Large-eddy simulation of wind-turbine wakes: Evaluation of turbine parametrisations," Boundary-Layer Meteorol. **138**, 345–366 (2011).
[7]M. Bastankhah and F. Porté-Agel, "A new analytical model for wind-turbine wakes," Renewable Energy **70**, 116–123 (2014).
[8]U. Högström, D. Asimakopoulos, H. Kambezidis, C. Helmis, and A. Smedman, "A field study of the wake behind a 2 mw wind turbine," Atmos. Environ. **22**, 803–820 (1988).
[9]R. J. Barthelmie, G. Larsen, S. Frandsen, L. Folkerts, K. Rados, S. Pryor, B. Lange, and G. Schepers, "Comparison of wake model simulations with offshore wind turbine wake profiles measured by sodar," J. Atmos. Ocean. Technol. **23**, 888–901 (2006).
[10]G. V. Iungo, Y.-T. Wu, and F. Porté-Agel, "Field measurements of wind turbine wakes with lidars," J. Atmos. Ocean. Technol. **30**, 274–287 (2013).
[11]M. Heisel, J. Hong, and M. Guala, "The spectral signature of wind turbine wake meandering: A wind tunnel and field-scale study," Wind Energy **21**, 715–731 (2018).
[12]J. Whale, C. G. Anderson, R. Bareiss, and S. Wagner, "An experimental and numerical study of the vortex structure in the wake of a wind turbine," J. Wind Eng. Ind. Aerodyn. **84**, 1–21 (2000).
[13]D. Medici and P. H. Alfredsson, "Measurements on a wind turbine wake: 3D effects and bluff body vortex shedding," Wind Energy **9**, 219–236 (2006).
[14]H. Snel, J. Schepers, and B. Montgomerie, "The Mexico project (model experiments in controlled conditions): The database and first results of data processing and interpretation," J Phys.: Conf. Ser. **75**, 012014 (2007).
[15]L. P. Chamorro and F. Porté-Agel, "A wind-tunnel investigation of wind-turbine wakes: Boundary-layer turbulence effects," Boundary-Layer Meteorol. **132**, 129–149 (2009).
[16]Global Wind Energy Council, "Annual Market Update 2017, Global Wind Report" (2017).
[17]W. Zhang, C. D. Markfort, and F. Porté-Agel, "Wind-turbine wakes in a convective boundary layer: A wind-tunnel study," Boundary-Layer Meteorol. **146**, 161–179 (2013).
[18]G. España, S. Aubrun, S. Loyer, and P. Devinant, "Wind tunnel study of the wake meandering downstream of a modelled wind turbine as an effect of large scale turbulent eddies," J. Wind Eng. Ind. Aerodyn. **101**, 24–33 (2012).
[19]L. P. Chamorro and F. Porté-Agel, "Effects of thermal stability and incoming boundary-layer flow characteristics on wind-turbine wakes: A wind-tunnel study," Boundary-Layer Meteorol. **136**, 515–533 (2010).
[20]Y.-T. Wu and F. Porté-Agel, "Atmospheric turbulence effects on wind-turbine wakes: An LES study," Energies **5**, 5340–5362 (2012).
[21]O. D. Vries, "On the theory of the horizontal-axis wind turbine," Annu. Rev. Fluid Mech. **15**, 77–96 (1983).
[22]H. Canet, P. Bortolotti, and C. L. Bottasso, "On the scaling of wind turbine rotors," Wind Energy Sci. **6**, 601–626 (2021).
[23]D. M. Eggleston and F. Stoddard, *Wind Turbine Engineering Design* (Van Nostrand Reinhold Co. Inc., New York, 1987).
[24]L. P. Chamorro, R. E. A. Arndt, and F. Sotiropoulos, "Reynolds number dependence of turbulence statistics in the wake of wind turbines," Wind Energy **15**, 733–742 (2012).
[25]D. Medici and P. H. Alfredsson, "Measurements behind model wind turbines: Further evidence of wake meandering," Wind Energy **11**, 211–217 (2008).
[26]M. Adaramola and P.-Å. Krogstad, "Experimental investigation of wake effects on wind turbine performance," Renewable Energy **36**, 2078–2086 (2011).
[27]F. Porté-Agel, Y.-T. Wu, H. Lu, and R. J. Conzemius, "Large-eddy simulation of atmospheric boundary layer flow through wind turbines and wind farms," J Wind Eng. Ind. Aerodyn. **99**, 154–168 (2011).
[28]L. Martinez, S. Leonardi, M. Churchfield, and P. Moriarty, "A comparison of actuator disk and actuator line wind turbine models and best practices for their use," AIAA Paper No. 2012-0900, 2012.
[29]J. N. Sørensen, R. F. Mikkelsen, D. S. Henningson, S. Ivanell, S. Sarmast, and S. J. Andersen, "Simulation of wind turbine wakes using the actuator line technique," Philos. Trans. R. Soc., A **373**, 20140071 (2015).
[30]L. J. Vermeer, J. N. Sørensen, and A. Crespo, "Wind turbine wake aerodynamics," Prog. Aerosp. Sci. **39**, 467–510 (2003).
[31]C. Wang, F. Campagnolo, H. Canet, D. J. Barreiro, and C. L. Bottasso, "How realistic are the wakes of scaled wind turbine models?," Wind Energy Sci. **6**, 961–981 (2021).
[32]P. Devinant, T. Laverne, and J. Hureau, "Experimental study of wind-turbine airfoil aerodynamics in high turbulence," J. Wind Eng. Ind. Aerodyn. **90**, 689–707 (2002).
[33]M. M. Alam, Y. Zhou, H. X. Yang, H. Guo, and J. Mi, "The ultra-low Reynolds number airfoil wake," Exp. Fluids **48**, 81–103 (2010).
[34]E. Llorente, A. Gorostidi, M. Jacobs, W. A. Timmer, X. Munduate, and O. Pires, "Wind tunnel tests of wind turbine airfoils at high Reynolds numbers," J. Phys.: Conf. Ser. **524**, 012012 (2014).
[35]O. Pires, X. Munduate, O. Ceyhan, M. Jacobs, and H. Snel, "Analysis of high Reynolds numbers effects on a wind turbine airfoil using 2D wind tunnel test data," J. Phys.: Conf. Ser. **753**, 022047 (2016).
[36]C. E. Brunner, J. Kiefer, M. O. L. Hansen, and M. Hultmark, "Study of Reynolds number effects on the aerodynamics of a moderately thick airfoil using a high-pressure wind tunnel," Exp. Fluids **62**, 1–17 (2021).
[37]I. Tani, "Boundary-layer transition," Annu. Rev. Fluid Mech. **1**, 169–196 (1969).
[38]R. Narasimha, "The laminar-turbulent transition zone in the boundary layer," Prog. Aerosp. Sci. **22**, 29–80 (1985).
[39]Y. S. Kachanov, "Physical mechanisms of laminar-boundary-layer transition," Annu. Rev. Fluid Mech. **26**, 411–482 (1994).
[40]Y. Lian and W. Shyy, "Laminar-turbulent transition of a low Reynolds number rigid or flexible airfoil," AIAA J. **45**, 1501–1513 (2007).
[41]A. J. Smits, B. J. McKeon, and I. Marusic, "High-Reynolds number wall turbulence," Annu. Rev. Fluid Mech. **43**, 353–375 (2011).
[42]M. Samie, I. Marusic, N. Hutchins, M. Fu, Y. Fan, M. Hultmark, and A. Smits, "Fully resolved measurements of turbulent boundary layer flows up to $Re_\tau = 20\,000$," J. Fluid Mech. **851**, 391–415 (2018).
[43]J. M. Jiménez, M. Hultmark, and A. J. Smits, "The intermediate wake of a body of revolution at high Reynolds numbers," J. Fluid Mech. **659**, 516–539 (2010).
[44]X. Yang, J. Hong, M. Barone, and F. Sotiropoulos, "Coherent dynamics in the rotor tip shear layer of utility-scale wind turbines," J. Fluid Mech. **804**, 90–115 (2016).

[45]F. Porté-Agel, M. Bastankhah, and S. Shamsoddin, "Wind-turbine and wind-farm flows: A review," Boundary-Layer Meteorol. **174**, 1–59 (2020).
[46]D. Micallef, C. S. Ferreira, T. Sant, and G. van Bussel, "Experimental and numerical investigation of tip vortex generation and evolution on horizontal axis wind turbines," Wind Energy **19**, 1485–1501 (2016).
[47]L. Lignarolo, D. Ragni, F. Scarano, C. Simão Ferreira, and G. van Bussel, "Tip-vortex instability and turbulent mixing in wind-turbine wakes," J. Fluid Mech. **781**, 467–493 (2015).
[48]S. Ivanell, R. Mikkelsen, J. N. Sørensen, and D. Henningson, "Stability analysis of the tip vortices of a wind turbine," Wind Energy **13**, 705–715 (2010).
[49]E. Kleusberg, S. Benard, and D. S. Henningson, "Tip-vortex breakdown of wind turbines subject to shear," Wind Energy **22**, 1789–1799 (2019).
[50]A. Piqué, M. A. Miller, and M. Hultmark, "Laboratory investigation of the near and intermediate wake of a wind turbine at very high Reynolds numbers," Exp. Fluids **63**, 106 (2022).
[51]D. Foti, X. Yang, M. Guala, and F. Sotiropoulos, "Wake meandering statistics of a model wind turbine: Insights gained by large eddy simulations," Phys. Rev. Fluids **1**, 044407 (2016).
[52]L. P. Chamorro, C. Hill, S. Morton, C. Ellis, R. E. A. Arndt, and F. Sotiropoulos, "On the interaction between a turbulent open channel flow and an axial-flow turbine," J. Fluid Mech. **716**, 658–670 (2013).
[53]R. Ashton, F. Viola, S. Camarri, F. Gallaire, and G. V. Iungo, "Hub vortex instability within wind turbine wakes: Effects of wind turbulence, loading conditions, and blade aerodynamics," Phys. Rev. Fluids **1**, 073603 (2016).
[54]F. Bingöl, J. Mann, and G. C. Larsen, "Light detection and ranging measurements of wake dynamics Part I: One-dimensional scanning," Wind Energy **13**, 51–61 (2010).
[55]F. Massouh and I. Dobrev, "Exploration of the vortex wake behind of wind turbine rotor," J. Phys.: Conf. Ser. **75**, 012036 (2007).
[56]N. Troldborg, J. N. Sorensen, and R. Mikkelsen, "Numerical simulations of wake characteristics of a wind turbine in uniform inflow," Wind Energy **13**, 86–99 (2010).
[57]Z. Yang, P. Sarkar, and H. Hu, "Visualization of the tip vortices in a wind turbine wake," J. Visualization **15**, 39–44 (2012).
[58]G. V. Iungo, F. Viola, S. Camarri, F. Porté-Agel, and F. Gallaire, "Linear stability analysis of wind turbine wakes performed on wind tunnel measurements," J. Fluid Mech. **737**, 499–526 (2013).
[59]M. Sherry, J. Sheridan, and D. L. Jacono, "Characterisation of a horizontal axis wind turbine's tip and root vortices," Exp. Fluids **54**, 1417 (2013).
[60]M. Ali and M. Abid, "Self-similar behaviour of a rotor wake vortex core," J. Fluid Mech. **740**, R1 (2014).
[61]N. Sedaghatizadeh, M. Arjomandi, R. Kelso, B. Cazzolato, and M. H. Ghayesh, "Modelling of wind turbine wake using large eddy simulation," Renewable Energy **115**, 1166–1176 (2018).
[62]D. Marten, C. O. Paschereit, X. Huang, M. Meinke, W. Schroeder, J. Mueller, and K. Oberleithner, "Predicting wind turbine wake breakdown using a free vortex wake code," AIAA J. **58**, 4672–4685 (2020).
[63]M. A. Miller, J. Kiefer, C. Westergaard, M. O. L. Hansen, and M. Hultmark, "Horizontal axis wind turbine testing at high Reynolds numbers," Phys. Rev. Fluids **4**, 110504 (2019).
[64]M. Vallikivi and A. J. Smits, "Fabrication and characterization of a novel nano-scale thermal anemometry probe," J. Microelectromech. Syst. **23**, 899–907 (2014).
[65]P. Welch, "The use of fast Fourier transform for the estimation of power spectra: A method based on time averaging over short, modified periodograms," IEEE Trans. Audio Electroacoust. **15**, 70–73 (1967).
[66]A. Piqué, M. A. Miller, and M. Hultmark, "Characterization of the wake behind a horizontal-axis wind turbine (HAWT) at very high Reynolds numbers," J. Phys.: Conf. Ser. **1618**, 062039 (2020).
[67]M. Felli and M. Falchi, "Propeller wake evolution mechanisms in oblique flow conditions," J. Fluid Mech. **845**, 520 (2018).
[68]S. Kang, X. Yang, and F. Sotiropoulos, "On the onset of wake meandering for an axial flow turbine in a turbulent open channel flow," J. Fluid Mech. **744**, 376–403 (2014).
[69]D. Medici and H. Alfredsson, "Wind turbine near wakes and comparisons to the wake behind a disc," in AIAA Paper No. AIAA 2005-595, 2005.
[70]V. L. Okulov, I. V. Naumov, R. F. Mikkelsen, I. K. Kabardin, and J. N. Sørensen, "A regular Strouhal number for large-scale instability in the far wake of a rotor," J. Fluid Mech. **747**, 369–380 (2014).
[71]F. Viola, G. V. Iungo, S. Camarri, F. Porté-Agel, and F. Gallaire, "Prediction of the hub vortex instability in a wind turbine wake: Stability analysis with eddy-viscosity models calibrated on wind tunnel data," J. Fluid Mech. **750**, R1 (2014).
[72]J. J. Miau, T. S. Leu, T. W. Liu, and J. H. Chou, "On vortex shedding behind a circular disk," Exp. Fluids **23**, 225–233 (1997).
[73]H. V. Fuchs, E. Mercker, and U. Michel, "Large-scale coherent structures in the wake of axisymmetric bodies," J. Fluid Mech. **93**, 185–207 (1979).
[74]J. B. Roberts, "Coherence measurements in an axisymmetric wake," AIAA J. **11**, 1569–1571 (1973).
[75]S. Cannon, F. Champagne, and A. Glezer, "Observations of large-scale structures in wakes behind axisymmetric bodies," Exp. Fluids **14**, 447–450 (1993).
[76]K. B. Howard, A. Singh, F. Sotiropoulos, and M. Guala, "On the statistics of wind turbine wake meandering: An experimental investigation," Phys. Fluids **27**, 075103 (2015).
[77]A. Segalini and P. H. Alfredsson, "A simplified vortex model of propeller and wind-turbine wakes," J. Fluid Mech. **725**, 91 (2013).
[78]S. Sarmast, A. Segalini, R. F. Mikkelsen, and S. Ivanell, "Comparison of the near-wake between actuator-line simulations and a simplified vortex model of a horizontal-axis wind turbine," Wind Energy **19**, 471–481 (2016).
[79]M. van der Laan, S. Andersen, M. Kelly, and M. Baungaard, "Fluid scaling laws of idealized wind farm simulations," J. Phys.: Conf. Ser. **1618**, 062018 (2020).